

## Research Article

**Cite this article:** Hassler M, Atasoy O, Twelker K, Kesler M, Birkendahl J, Krammer J (2020). A comparison on simulated, analytic, and measured impedance values for an inductive power transfer system. *Wireless Power Transfer* 7, 51–59. <https://doi.org/10.1017/wpt.2020.6>

Received: 29 August 2019  
Revised: 13 January 2020  
Accepted: 14 January 2020  
First published online: 19 February 2020


**Keywords:**

Impedance measurement; IPT; IPTS; SAE J2954; WPT

**Author for correspondence:**

Marius Hassler, BMW Group, 80788 Munich, Germany.  
E-mail: [marius.hassler@bmw.de](mailto:marius.hassler@bmw.de)

# A comparison on simulated, analytic, and measured impedance values for an inductive power transfer system

Marius Hassler<sup>1,2</sup> , Oguz Atasoy<sup>3</sup>, Karl Twelker<sup>3</sup>, Morris Kesler<sup>3</sup>, Johannes Birkendahl<sup>2</sup> and Josef Krammer<sup>1</sup>

<sup>1</sup>BMW Group, 80788 Munich, Germany; <sup>2</sup>Technical University of Munich, Arcisstr. 21, 80333 Munich, Germany and <sup>3</sup>WitTricity Corporation, MA 02472 Watertown, USA

**Abstract**

Studies on inductive power transfer (IPT) systems are most times either theoretical or experimental. In this paper, we want to bring theoretical models and experimental data together using the impedance based interface proposed in SAE J2954. This proposal characterizes the IPT system by impedances at both coil terminals. We show how the experimental data was retrieved at the interface and use it to validate an analytical model and a Simulink model described within this study. Such models can support the design and development process and therefore a comparison with reality is necessary.

**Introduction**

Recently, German car manufacturer Daimler, Porsche, and VW announced that the fleet share of electrified vehicles is projected to be 50% in 2030 [1–3]. With every second car becoming electric, the rising number of electric vehicle (EV) users will ask for a more convenient way of charging than conventional wired charging, which requires them to plug in regularly. The chore of handling the charging cable, connecting to – and disconnecting from – the socket can be spared by wireless charging. A comfort charging solution that starts automatically when a vehicle is parked above a charging system to recharge the EV battery. The automatic recharging with a 11 kW system can reestablish around 440 km of range when charging for 8 h during work or overnight, assuming an EV driving consumption rate of 20 kWh per 100 km, covering the majority of regularly needed user ranges [4]. In order that customers with EVs from different OEMs can use the same infrastructure to recharge their vehicles, the SAE is elaborating a technical standard called “Wireless Power Transfer for Light-Duty Plug-In/Electric Vehicles and Alignment Methodology” (J2954) [5]. The standard and [6] proposed to use an impedance based interface to characterize the system behavior due to the interdependency of vehicle assembly (VA) and ground assembly (GA) coils. Yet, there existed no measurement device that is capable to measure the impedance with acceptable precision. For this reason, [7] developed a methodology consisting of current and voltage measurements in an impedance matching network and a calculation theory that make the precise impedance measurement during power transfer possible. Their results show impedance uncertainties reduced by factor 6 – 34 from above 1  $\Omega$  to around 0.1  $\Omega$  in average, depending on the measurement parameters.

With real impedance measurement data available, the possibility to validate simulation models arose and provide an answer to the question “Do measurement and simulation agree?”

In this paper, we present an analytic model and a *Simulink* model. Both models will be compared with each other and with the measured impedance values. Such models can be applied to support the design and development of interoperable inductive charging systems. However, validation and comparison of a model with the reality are essential for further improvements. It is also an important step towards virtual validation of interoperability of inductive power transfer systems. In the paper, we’ll also present how an impedance measurement can be integrated in a *Simulink* simulation and what a control loop may look like.

**Method**

This section introduces two different simulation models, an analytical and a *Simulink* model, which will be compared within this study. The simulation models are used to simulate the impedance at the VA interface that is defined at the VA coil terminals as illustrated in Fig. 1. The electric parameters of the electromagnetic coupler  $L_{GA}$ ,  $L_{VA}$ , and  $M$  will be measured in the experimental setup by a vector network analyzer (VNA) to achieve high precision [8–10]. Of course, these parameters could also be calculated by means of FEM simulation, but

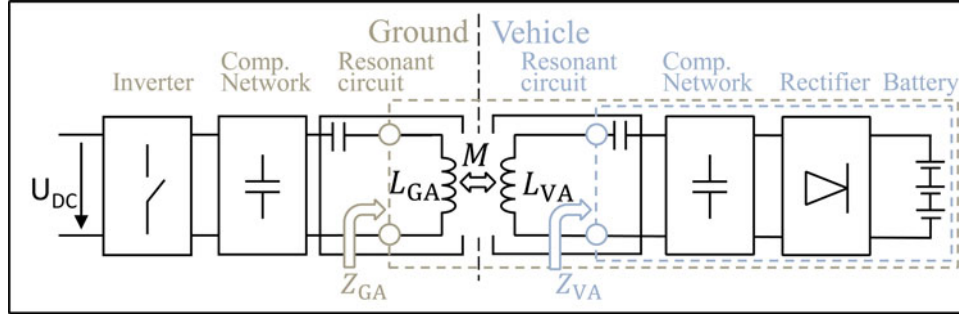


Fig. 1. Block diagram of an inductive charging system [6].

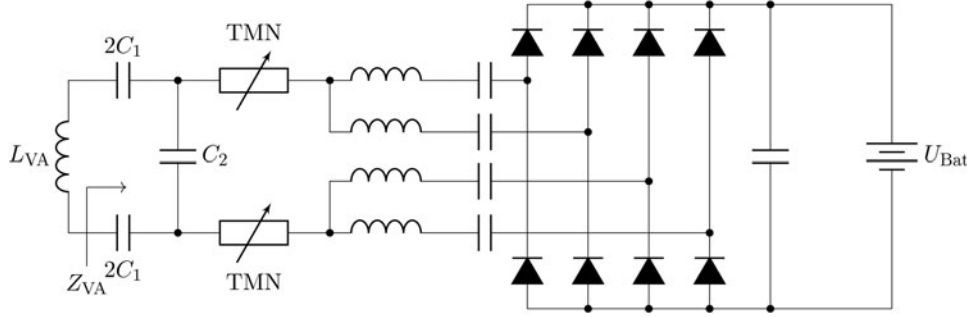


Fig. 2. Example of a VA circuit from SAE J2954 [5].

this would require many iterative steps to adapt the simulation model until it represents the real system with adequate agreement [11, 12]. The measurement is performed for each offset position, where offset denotes a vertical and horizontal displacement ( $x, y, z$ ) between VA coil and GA coil centers. The relevant impedance at the GA interface  $Z_{GA}$  for VA characterization is then calculated with the obtained data from the simulation model ( $Z_{VA}$ ) and the data from the VNA-measurement using

$$Z_{GA} = R_{GA} + j\omega L_{GA} + \frac{\omega^2 M^2}{R_{VA} + j\omega L_{VA} + Z_{VA}}, \quad (1)$$

where  $\omega$  is the angular frequency.  $R_{GA}$  and  $R_{VA}$  are the coil resistances. These resistances can be difficult to measure directly but can be determined from the quality factors of the coils using  $R_{xA} = \omega L_{xA}/Q_{xA}$ . The quality factor is a function of relative coil position, and was not measured at all positions, so for this work we assume  $Q_{xA} = 400$ .

### Analytic model

For a first approximation of the VA impedance of the circuit shown in Fig. 2, we use a simple analytic model that implements the functionality of the circuit and neglects any nonlinear behavior and phase changes. We assume the rectifier input current  $I_{rect}^{in}$  in each branch to be sinusoidal and the rectified current  $I_{Bat}$  to be constant. Using the average of the rectified sine waves in the parallel branches, we can write

$$I_{Bat} = \frac{4}{\pi} I_{rect}^{in}, \quad (2)$$

and introduce the simplified equivalent circuit model presented in Fig. 3, where  $X$  comprises the rectifier input filter inductance and

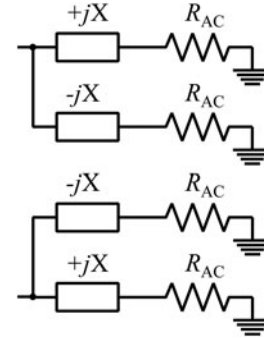


Fig. 3. Equivalent circuit model of Fig. 2 rectifier for analytic calculations.

capacitance. The AC equivalent load resistance in each branch can be mathematically described using the Steigerwald approximation [13]

$$R_{AC} = \frac{8}{\pi^2} \frac{U_{Bat}^2}{P_{out}}. \quad (3)$$

Subsequent, the rectifier input impedance can be summarized to

$$Z_{rect} = \frac{X^2 + R_{AC}^2}{R_{AC}}, \quad (4)$$

a purely real impedance whose imaginary part cancels out.

The impedance at the VA coil terminals can be derived to

$$Z_{VA} = \frac{1}{j\omega C_1} + \frac{(1/j\omega C_2) \cdot (Z_{TMN} + Z_{rect})}{(1/j\omega C_2) + Z_{TMN} + Z_{rect}}, \quad (5)$$

with  $Z_{TMN}$  being the impedance of the tunable matching network (TMN) that can be set to take any impedance value from  $[0, -24] j\Omega$ .

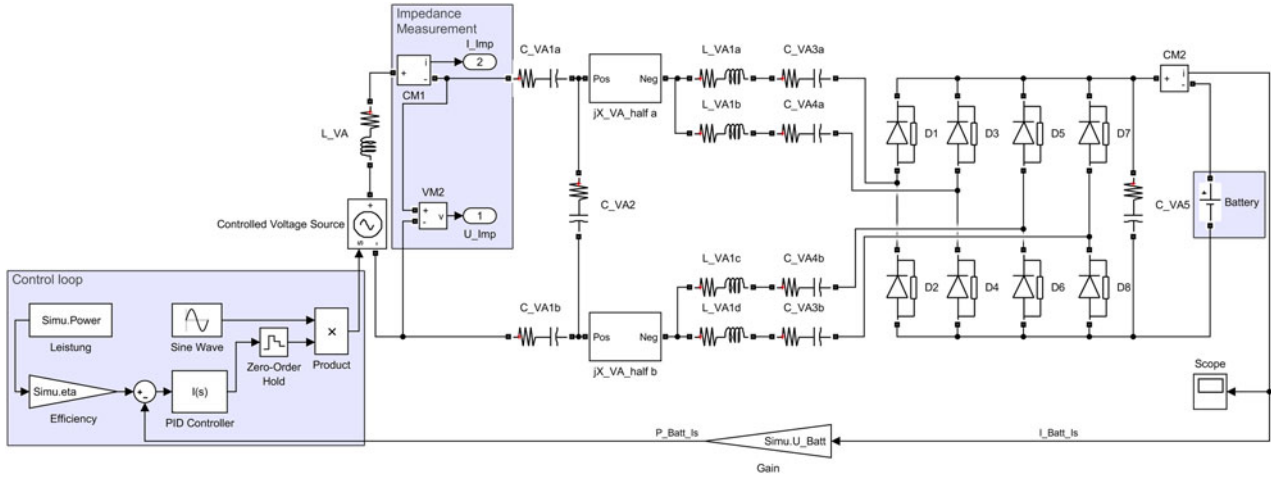


Fig. 4. Simulink simulation model.

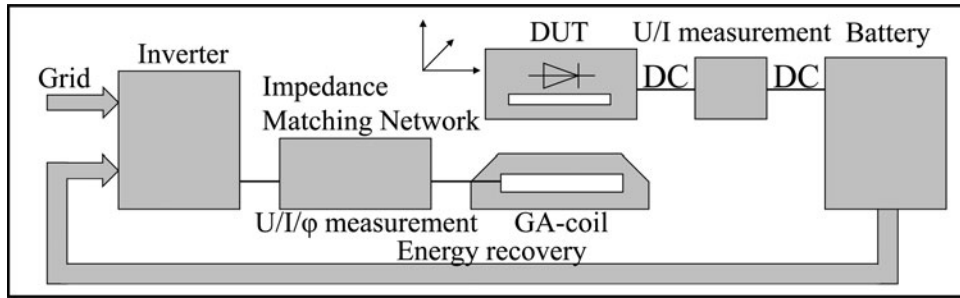


Fig. 5. Schematic impedance measurement setup [7].

**Simulink model**

The characterization of a system across different states requires a sophisticated simulation model capable of handling different battery voltages, different power levels, frequencies, and – if existing – different states of active circuit components. Therefore, a *Simulink* model is well suited. In *Simulink*, it is more convenient – compared to other simulation tools like *LTspice* – to implement a control loop that ensures that the same amount of power is transferred to the battery across different parameter sweeps, making automatization of the simulation model much easier.

The circuit illustrated in Fig. 2 is characterized by the impedance at the VA coil terminals,  $Z_{VA}$ . As the GA coil current is sinusoidal, we may reduce the simulation model and omit the GA circuit, which has no effect on the impedance outcome. Instead, we apply a sinusoidal voltage source that represents the induced voltage into the VA circuit. The voltage source amplitude

$$U_{VA}^{ind} = \omega M I_{GA}, \tag{6}$$

is steered by the control loop that ensures a certain amount of power at the battery. Sensors VM2 and CM1 (cf. Fig. 4) measure the voltage and current needed to calculate the impedance  $Z_{VA}$ .

**Simulink impedance measurement**

To retrieve the impedance from *Simulink* simulations, it is required to convert the direct observable time signal of current and voltage

into a frequency-dependent impedance value. Whenever the time signal deviates from a purely sinusoidal waveform, it contains harmonic contributions. To filter out these harmonic contents that do not contribute to the energy transfer, we apply a Fourier analysis. The impedance for the fundamental frequency averaged over one period can be calculated using the following identity [14]

$$a_n = 2f_0 \int_0^T f(t) \cdot \cos(n\omega t) dt, \tag{7}$$

$$b_n = 2f_0 \int_0^T f(t) \cdot \sin(n\omega t) dt.$$

This divides the time signal into its cosine and sine components. Inserting  $n=1$  into equation (7) yields the fundamental component.

The impedance is then given by

$$|Z| = \frac{\sqrt{a_{1,u}^2 + b_{1,u}^2}}{\sqrt{a_{1,i}^2 + b_{1,i}^2}}, \tag{8}$$

and the phase difference between voltage and current is

$$\varphi_{UI} = \tan^{-1}\left(\frac{a_{1,u}}{b_{1,u}}\right) - \tan^{-1}\left(\frac{a_{1,i}}{b_{1,i}}\right). \tag{9}$$

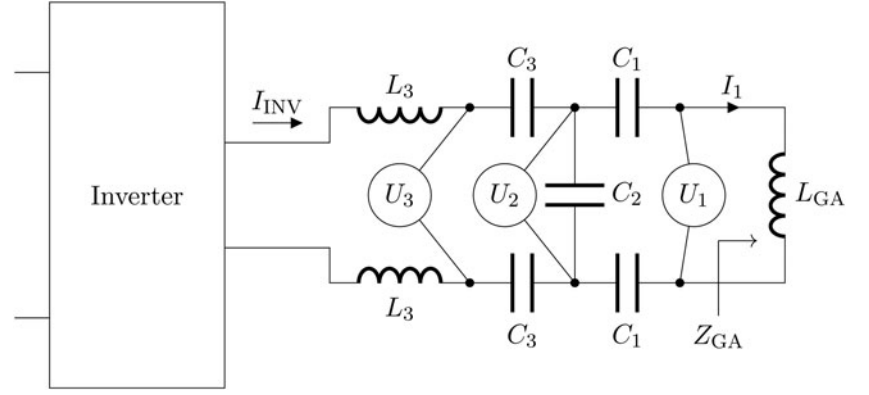


**Fig. 6.** Schematics of the impedance measurement device with three voltage and one current measurement position.

**Table 1.** Correction parameters [7]

$a_{c_1}$	$a_{c_2}$	$a_{c_3}$	$a_{u_1}$	$a_{u_2}$	$a_{u_3}$
0.980	0.993	1.007	0.990	0.980	0.991
$a_{I_1}$	$b_{\varphi_{u_1}} [^\circ]$	$b_{\varphi_{u_2}} [^\circ]$	$b_{\varphi_{u_1}} [^\circ]$	$b_{\varphi_{u_1} u_3} [^\circ]$	$b_{\varphi_{u_2} u_3} [^\circ]$
0.970	1.102	-0.688	-1.788	-1.742	0.040

**Table 2.** Coil parameter uncertainty assumption

$\Delta L_{GA}$ [%]	$\Delta L_{VA}$ [%]	$\Delta k$ [%]
3	3	3

### Measurement setup

The measurement setup is based on the proposal of [5, 6]. The first measurement results show that a significant improvement in comparison with the direct voltage–current (UI) method can be achieved [7]. The setup is illustrated in Fig. 5. Testing different VAs in different positions, different power levels, and in different settings on the same setup requires the inverter and the impedance matching network to handle a wide range of impedances. We therefore utilize a special laboratory inverter<sup>1</sup> that can support a wide range of inductive loads and a special impedance matching network that maximizes the supported range of presented impedances at the GA coil terminals. The presented impedance comprises the primary coil impedance and the reflected vehicle system impedance, which are both offset dependent.

The schematics of the impedance matching network and the measurement ports are illustrated in Fig. 6. The device under test is integrated in a test robot that ensures high positioning accuracy and reproducibility. Its direct current (DC) output is connected with a controllable DC load that presents the set battery voltage. The received energy is recovered and reused for the DC source.

The measurands  $U_1$ ,  $U_2$ ,  $U_3$ ,  $I_1$ ,  $P_{in}$ ,  $P_{out}$  and their respective phases are used to calculate the impedance at the primary coil terminal in different ways ( $Z_{GA,i}$ ). A perfect measurement set up would yield a cluster of points, each calculated differently, at the same  $Z_{GA}$  impedance. However, real world measurements are subject to measurement errors and thus deviate from perfect.

To compensate for constant, systematic errors, we apply a fit in the form of  $a \cdot x$  for the measurands and in the form of  $b \pm x$  for the phases. The fit is applied across a large number of measurements and yields the correction parameters shown in Table 1 that minimize the measurement error. More details are presented in [7]. There, also the process of selecting the right correction parameters is given.

The impedance  $Z_{GA}$  is calculated by means of a weighted mean function

$$Z_{GA_{mean}} = \frac{\sum_{i=1}^N g_i \cdot Z_{GA,i}}{\sum_{i=1}^N g_i}, \quad (10)$$

which weighs each contributing function with its uncertainty  $g_i = (\Delta Z_{GA,i})^{-2}$  according to Gaussian error propagation [15].

### Coil parameter measurement

Measuring the coil parameters  $L_{GA}$ ,  $L_{VA}$ , and  $k$ , can be straightforward during the development process. However, once a VA design is optimized towards automotive requirements and becomes more like a production ready product, it may no longer be possible to make such measurements directly, e.g. the capacitors may be integrated into the coil assembly and no longer be detachable – which would be required for a VNA measurement. For this reason, we measured the coil parameters before the final assembly with a VNA for different coil offset positions. These measurements were made using a custom-built computer-controlled positioning device, constructed from 80/20 aluminum extrusion. All aluminum extrusions supporting the VA assembly are positioned far from the power transfer coils to avoid affecting the measurements. These measurements use the same 1.1 m × 1.1 m aluminum plate used in the power transfer measurements. More details on the test setup can be found in [5].

However, those positions may not be identical to those used in the impedance measurement setup, and the final assembly of the VA coil can result in some changes to coil properties.

<sup>1</sup>Inverter details:  $U_{DC} = [100, 600]$  V,  $I_{out,max} = 100$  A,  $\varphi = [0^\circ, 70^\circ]$ ,  $f = [80, 90]$  kHz.

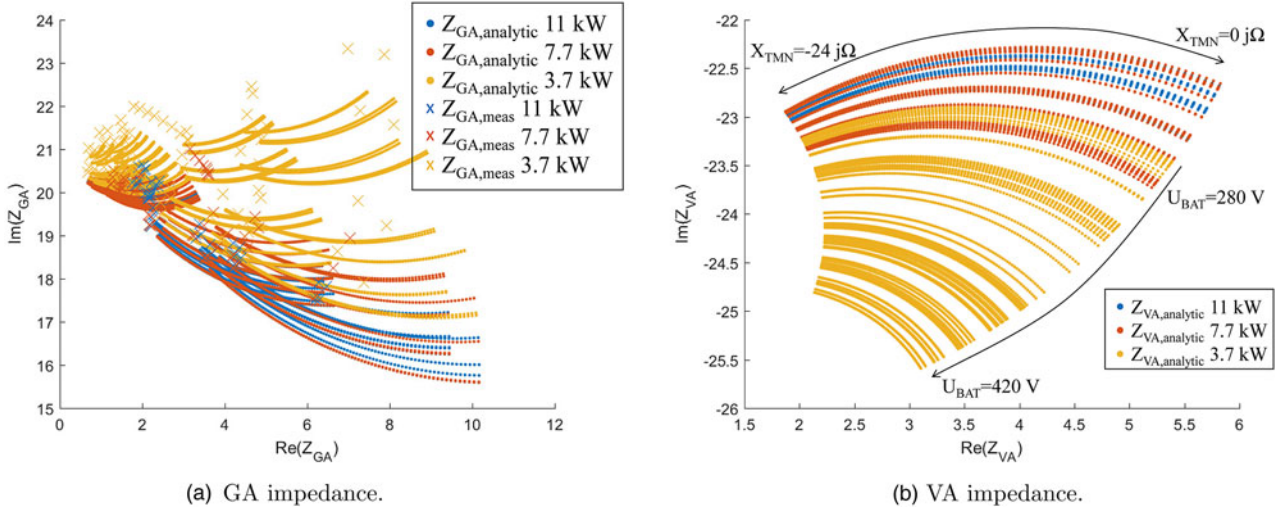


Fig. 7. GA and VA impedance for WPT3 SAE J2954 Reference VA from [5] calculated with the analytic model.

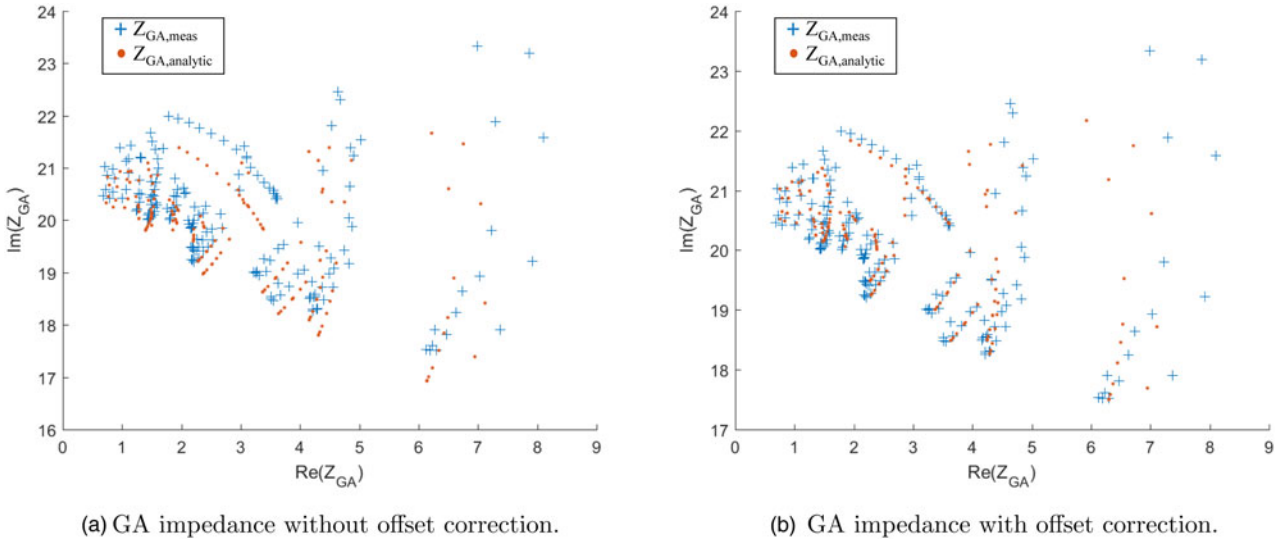


Fig. 8. GA impedance before and after offset correction for the analytic model.

Consequently, there is some uncertainty in the coil parameter values that must be accounted for in addition to the measurement uncertainty originating from the VNA. To account for the possibly introduced offsets, we apply a fit for each position within the assumed uncertainty ranges depicted in Table 2. Numerous measurements were made at each position to help reduce uncertainty.

**Results and discussion**

First, the results for each method will be presented individually, then a comparison between each model and the real measurement data is drawn. To be able to compare the results, we use the measurement output data  $P_{out}$  and  $U_{Bat}$  as inputs for both models. The measurement was performed for the set of conditions

$$\begin{aligned}
 U_{bat} &= \{280, 320, 380, 420\}V, \\
 P_{in} &= \{3.7, 7.7, 11\}kW, \\
 (x, y) &= (0, 0), (0, 100), (75, 0), (75, 100)mm, \\
 z &= 140, 210 \text{ mm},
 \end{aligned}
 \tag{11}$$

and for different states of the active component in the VA circuit (c.f. Fig. 2), the so called TMN.

**Analytic model results**

With equation (5) the impedance for the analytic model  $Z_{VA,analytic}$  can be calculated. The TMN function is incorporated by a parameter sweep of  $Z_{TMN}$  that adds one dimension to the impedance vector  $Z_{VA}$ . The result is shown in Fig. 7(b). The GA impedance is calculated by inserting the VA impedance into equation (1). The result is shown in Fig. 7(a).

As seen in Fig. 7(b), the TMN reactance provides a means to vary the VA impedance. During operation, due to different system constraints, for example, coil current limitations, voltage limits, etc., it may not be possible to achieve the desired power over the full TMN reactance range (nor would it be necessary). As a result, in the measurements reported here the TMN reactance values were limited to those at which the desired power could be reached. The TMN reactance value was adjusted from a control computer via a graphical user interface (GUI).

**Table 3.** Offset correction parameters for analytically calculated  $Z_{GA}$ 

$x$ [mm]	$y$ [mm]	$z$ [mm]	$L_{GA}$ [ $\mu$ H]	$L_{VA}$ [ $\mu$ H]	$k$	$a_{L_{GA}}$	$a_{L_{VA}}$	$a_k$	$\varepsilon_{(xyz)}$ [ $\Omega$ ]
75	100	140	36.6	44.0	0.170	1.01	0.993	0.993	0.196
0	100	140	35.8	44.1	0.210	1.02	0.993	0.993	0.284
75	0	140	36.1	44.0	0.175	1.01	0.993	0.979	0.209
0	0	140	35.1	44.1	0.221	1.01	0.999	0.993	0.354
75	100	210	37.9	43.1	0.089	1.01	0.994	1.02	0.090
0	100	210	37.7	43.1	0.108	1.01	0.997	0.992	0.104
75	0	210	37.8	43.1	0.097	1.01	1.00	0.985	0.099
0	0	210	37.5	43.2	0.118	1.02	0.993	1.03	0.165

**Table 4.** Deviation between real data and analytic model for different power levels

$\varepsilon_{3.7kW}$ [ $\Omega$ ]	$\varepsilon_{7.7kW}$ [ $\Omega$ ]	$\varepsilon_{11kW}$ [ $\Omega$ ]
0.294	0.107	0.132

The control value of the TMN setting in the GUI is not directly the reactance of the element, and since the TMN was being used as a “black box”, it was required to come up with a mapping for use in the analytical model. The mapping was developed using the constraints that the TMN value should be in the range  $[0 - 24]$   $j\Omega$  and that the same TMN setting from any measurement must also show the same  $Z_{TMN}$  value. For the arbitrary mappings, the one  $Z_{TMN}$  value that yields the lowest overall deviation was chosen. The result of the mapping between TMN GUI setting and reactance value agrees well with our expectation.

In Fig. 8(a) the results with the above described TMN selection process are shown. It can be directly seen that the analytically calculated  $Z_{GA,analytic}$  and the measured impedances  $Z_{GA,mean}$  share a similar shape and are in close proximity. However, we also see that there are deviations. These deviations could be the result of differences in  $L_{GA}$ ,  $L_{VA}$ , and  $M$  between the tested GA and VA coils and the VNA measurements made before final assembly as well as any differences in the coil position between the same. This can be investigated by looking at different parameters of the electromagnetic coupler within the assumed uncertainty parameters depicted in Table 2. We therefore setup a fit that minimizes the Euclidean distance  $\varepsilon$  between the measured and the respective analytically calculated impedances. We assume that the high number of measurements can be used to correct for any systematic errors in the positioning. Figure 8(b) shows the result. For a better visualization we omitted the power dependent color coding. The applied correction parameters are given in Table 3.

It can be seen that the offsets could be clearly reduced through this correction process. This is also shown by the mean deviation  $\bar{\varepsilon}$  which could be reduced by more than a factor of two from 0.439 to 0.190  $\Omega$ . However, there are some points with high real part corresponding to 3.7 kW that differ from the measurement data. Looking at the deviation across different power levels, we see in Table 4 that the deviation for 3.7 kW is around 3 times more than for higher power levels.

### Simulink model results

The impedance  $Z_{VA,simulink}$  was computed as indicated in Fig. 4 by applying the method presented in (1) to retrieve its impedance. The VA impedance is shown in Fig. 9(b). For the mapping onto the GA interface, we also apply equation (1) and the measured coil parameters. Figure 9(a) shows the resulting calculated impedances  $Z_{GA,simulink}$ . Similar to the analytic model, the VA and GA impedance also includes a parameter sweep of the TMN. For this reason, we apply the same selection process as used for the analytic model. Subsequent, we correct for systematic errors in the positioning by means of a fit that minimizes the Euclidean distance between the measured and the respective simulated impedances. The result is shown in Fig. 10. The applied correction factors are given in Table 5. The mean deviation  $\bar{\varepsilon}$  between measured and simulated impedances can approximately be halved from 0.619 to 0.304  $\Omega$  with the correction process. The deviation across different power levels is given in Table 6. It also shows a better agreement for 11 and 7.7 kW and worse for 3.7 kW case. This could be from temperature dependent resistance effects of the SiC-diodes at higher power levels that were not implemented in the *Simulink* model but might meet the assumed resistance values better.

### Discussion

At the beginning of this study, we had the expectation that the simple analytic model would deviate more from the measurements than the *Simulink* model. However, the results show the opposite finding. The analytic model – based on Steigerwalds’ approximation – agrees well with the measurement results and the results obtained with the *Simulink* model do not. Of course, the reason is not the *Simulink* tool itself. Instead, there has to be a deviation between the simulated model and the actual VA. We traced the major difference back to the rectifier input impedance. The rectifier impedance contains no imaginary impedance in the analytic model. This is quite different in the case of the *Simulink* model, based on a time-domain circuit simulation, where the rectifier impedance contains a capacitive reactance. This is due to nonlinear effects of the diodes that are not yet well understood and subject of future research. Further errors in the simulation model could be introduced by the unknown TMN, component deviations from specified values, or temperature effects. Further improvement in the agreement between the simulation model and measurement data has not yet been

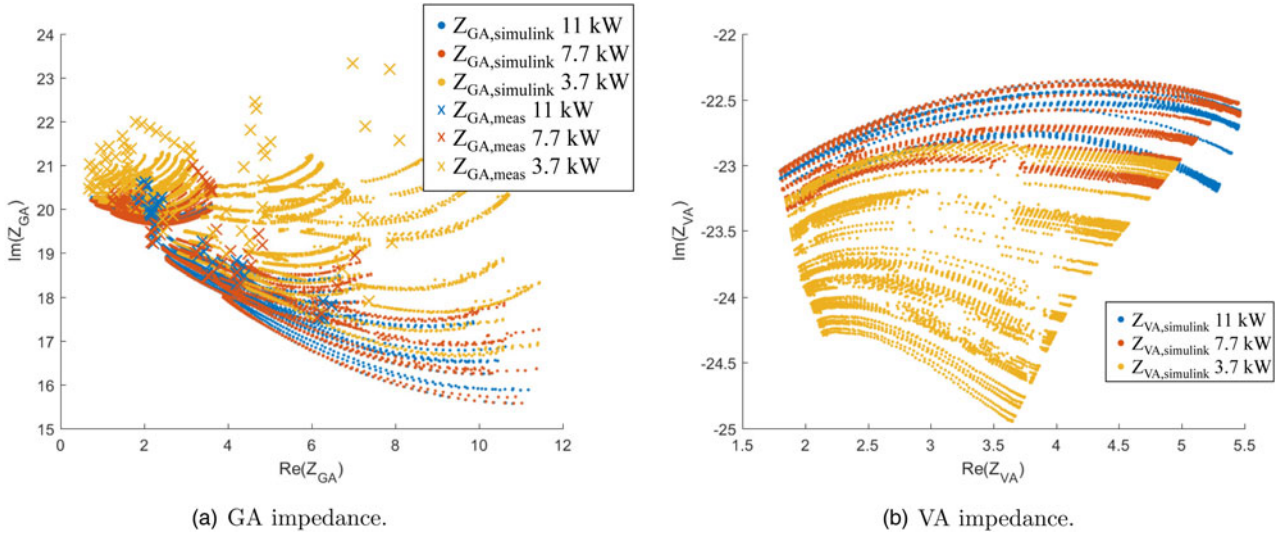


Fig. 9. GA and VA impedance for WPT3 SAE J2954 Reference VA from [5] calculated with the *Simulink* model.

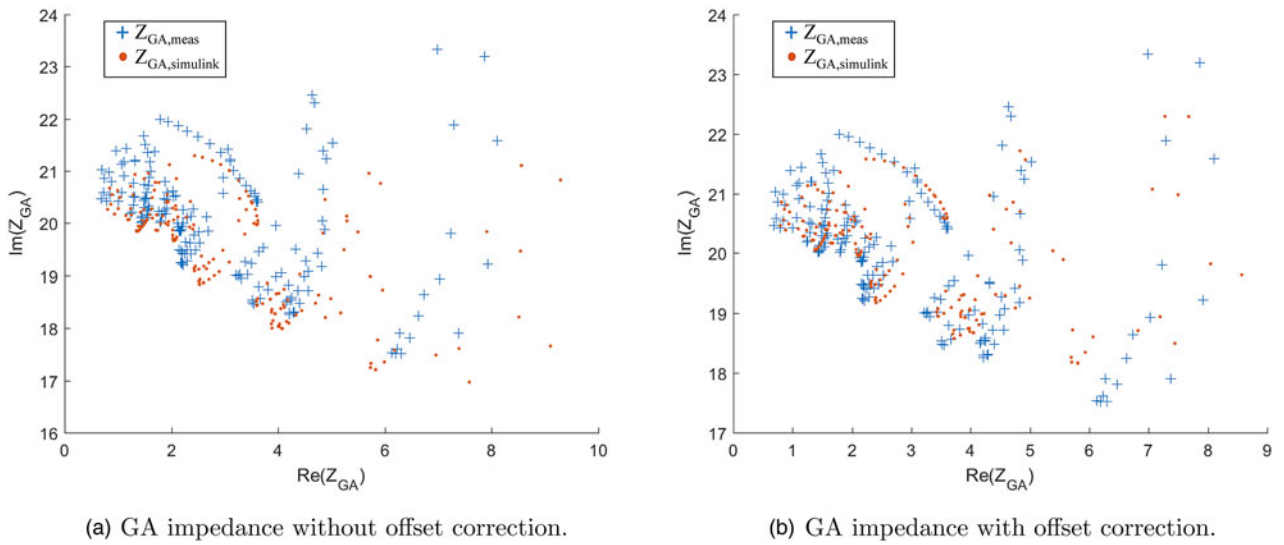


Fig. 10. GA impedance before and after offset correction for the *Simulink* model.

Table 5. Offset correction parameters for simulated  $Z_{GA}$

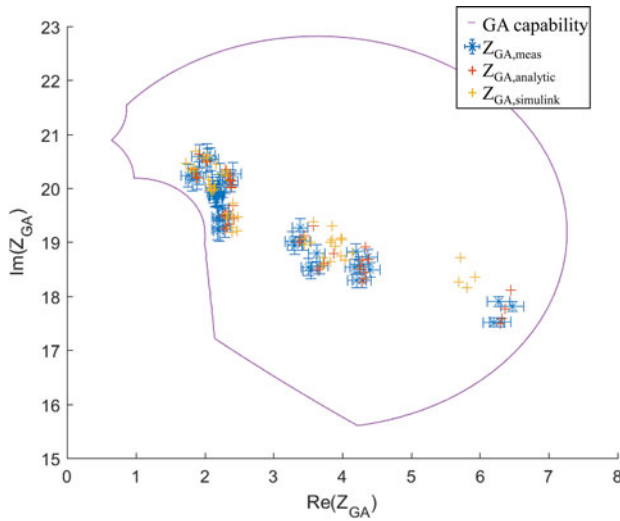
$x$ [mm]	$y$ [mm]	$z$ [mm]	$L_{GA}$ [ $\mu$ H]	$L_{VA}$ [ $\mu$ H]	$k$	$a_{LGA}$	$a_{LVA}$	$a_k$	$\epsilon_{(xyz)}$ [ $\Omega$ ]
75	100	140	36.6	44.0	0.170	1.01	0.984	0.970	0.351
0	100	140	35.8	44.1	0.210	1.01	0.984	0.970	0.513
75	0	140	36.1	44.0	0.175	1.01	0.982	0.970	0.372
0	0	140	35.1	44.1	0.221	1.01	0.980	0.970	0.403
75	100	210	37.9	43.1	0.089	1.01	0.996	0.989	0.151
0	100	210	37.7	43.1	0.108	1.01	0.995	0.972	0.193
75	0	210	37.8	43.1	0.097	1.01	0.991	0.970	0.170
0	0	210	37.5	43.2	0.118	1.01	0.990	1.01	0.235

**Table 6.** Deviation between real data and *Simulink* model for different power levels

$\varepsilon_{3.7\text{kW}} [\Omega]$	$\varepsilon_{7.7\text{kW}} [\Omega]$	$\varepsilon_{11\text{kW}} [\Omega]$
0.399	0.211	0.272

**Table 7.** Inverter assumptions used to calculate GA electronic capability

	$I_{\text{inv}} [\text{A}]$	$U_{\text{inv}} [\text{V}]$	$\varphi_{\text{inv}} [^\circ]$	$P_{\text{GA}} [\text{kW}]$
Min	20	380	0	11
Max	40	500	45	

**Fig. 11.** Calculated, simulated, and measured impedance  $Z_{\text{GA}}$  with WPT3 reference GA electronics capability from [5]. All impedances within the purple envelope correspond to different EV operation points that can be powered with 11 kW.

successful and needs further investigation. Therefore, we recommend the use of the analytical model for design purposes. However, for qualifying product VAs and ensuring standard conformity, impedance measurements are indispensable.

To determine if the circular WPT3 reference GA from SAE J2954 [5] is capable of driving the calculated and measured impedance values that characterize the WPT3 VA depicted in Fig. 2, we take the inverter assumptions given in Table 7 and calculate its impedance at the GA interface.

The result is shown in Fig. 11 with calculated, simulated, and the measured impedance values for the different operating points at 11 kW. The measured impedance values are also shown with their uncertainty. The mean uncertainty is  $0.113 \Omega + 0.176 \text{ j}\Omega$ . The GA electronics of the reference WPT3 GA from SAE J2954 can achieve 11 kW output power with all impedances inside the purple envelope. This shows that this method is well suited for the design development process indicating compatibility of VA and GA, or GA impedance and GA electronics. The feedback from impedance measurements can also be applied to improve the simulation models for better prediction capability.

## Conclusion

In this paper, we presented two methods to analyze inductive power transfer systems: an analytic model and a *Simulink*

model. We compared the theoretical values of both methods with the first impedance measurement results on IPT systems. On the way, we encountered a product challenge – differences in the coil parameters originating from the difference between the pre-assembly coil characterization and the impedance measurement positions. This problem could be solved by means of a fit that minimizes the error in each position. We assume that the systematic errors cancel out when having several different measurement settings for each position and did not corrupt the data. The results show that both models achieve a similar shape in close proximity to the measured values even before offset correction. However, the analytically calculated impedances  $Z_{\text{GA},\text{analytic}}$  show a better agreement with the measurement results. In both cases, the agreement is better for 7.7 and 11 kW than for 3.7 kW. The proposed method to describe IPT systems is a way to specify and to test the compatibility of the energy transfer with few additional definitions and as a consequence, with little additional test machinery. One of the key features is to use the geometric definitions of standard coil systems as a reference. Hence the method is tied closely to the definition of the standard. Nevertheless, the technique and underlying calculations are challenging and additional VA systems need to be measured, simulated, and compared for a better understanding.

## References

- [1] Preuss S. Daimler plant CO2-Wende: Bis 2030 soll jeder zweite Mercedes elektrisch sein, FAZ.NET, [Online]. Available at <https://www.faz.net/aktuell/wirtschaft/auto-verkehr/daimler-bis-2030-soll-jeder-zweite-mercedes-elektrisch-sein-16184951.html>. (Accessed 14 June 2019).
- [2] Kreimeier N. Dr. Volks und Mr. Wagen, Capital.de, [Online]. Available at <https://www.capital.de/wirtschaft-politik/dr-volks-und-mr-wagen>. Accessed 12 June 2019).
- [3] Freitag M. Porsche plant mit Elektroanteil von 50 Prozent schon in sechs Jahren, manager magazin, [Online]. Available at <https://www.manager-magazin.de/unternehmen/autoindustrie/porsche-jedes-zweite-fahrzeug-soll-bald-elektroauto-sein-a-1153417.html>. (Accessed 12 June 2019).
- [4] U.S. Department of Transportation: 2009 National Household Travel Survey, 2009.
- [5] Wireless Power Transfer for Light-Duty Plug-In/Electric Vehicles and Alignment Methodology, SAE J2954 RP, 2017.
- [6] Hassler M, Niedermeier F, Krammer J and Diepold K (2018) A Method for Interoperable Interface Description of Inductive Power Transfer Systems, 2018 IEEE PELS Workshop on Emerging Technologies: Wireless Power Transfer (Wow), Montréal (Canada).
- [7] Hassler M, Atasoy O, Kesler M, Twelker K, Achatz T, Jetz M and Krammer J (2019) Impedance Measurement on Inductive Power Transfer Systems, 2019 IEEE PELS Workshop on Emerging Technologies: Wireless Power Transfer (Wow), London (GB).
- [8] Auvigne CB (2015) Electrical and Magnetical Modeling of Inductive Coupled Power Transfer Systems, EPFL.
- [9] Cirimele V (2017) Projet et intégration d'un système de transfert inductif pour les applications automobiles.
- [10] Esteban B, Sid-Ahmed M and Kar NC (2015) A comparative study of power supply architectures in wireless EV charging systems. *IEEE Transactions on Power Electronics* 30, 6408–6422.
- [11] Niedermeier F (2019) Methoden zur Analyse von induktiven Ladesystemen für Elektro- und Hybridfahrzeuge.
- [12] Kürschner D and Rathge C (2008) Contactless energy transmission systems with improved coil positioning flexibility for high power applications, 2008 IEEE Power Electronics Specialists Conference, Rhodes (Greece).
- [13] Steigerwald RL (1988) A comparison of half-bridge resonant converter topologies. *IEEE Transactions on Power Electronics* 3, 174–182.



- [14] **Unbehauen R** (1994) *Grundlagen der Elektrotechnik – Allgemeine Grundlagen, Lineare Netzwerke, Stationäres Verhalten*. Heidelberg, Berlin: Springer.
- [15] **Gupta SV** (2012) *Measurement Uncertainties: Physical Parameters and Calibration of Instruments*. Heidelberg, Berlin: Springer.



**Marius Hassler** received his B.Sc. and M.Sc. degree in physics with specialization in condensed matter from the Technical University of Munich, Germany. He is currently working toward the Dr.-Ing. degree in engineering with BMW Group, from the Technical University of Munich, Germany. His current research interests include circuit simulation and inductive charging.



**Oguz Atasoy**, Ph.D. is working as a senior staff scientist at Witricity Corporation. His tasks include the design, development, and improvement of wireless power solutions. His work at Witricity leads to patent applications as well as conference publications. He received his Ph.D. from EPFL (Swiss Institute of Technology Lausanne) in Microsystems and Microelectronics, and his MSc and BSc in Electrical and Electronics Engineering from Bogazici University, Turkey.



**Karl Twelker** received his Ph.D. in experimental neutrino physics from Stanford University in 2014. He joined WiTricity Corporation in 2015 to work on wireless power systems for automotive and consumer electronics applications. He is now at The Charles Stark Draper Laboratory, Inc.



**Morris Kesler** is the Chief Technology Officer at WiTricity Corporation where he is responsible for the research and development activities in the company. He joined WiTricity in 2007 and has served as Chief Engineer and vice president of research and development. Prior to joining WiTricity, he was a founder of Wide Net Technologies, Inc., which developed unique optical communication and sensing systems for both government and industry, and a Consulting Engineer at PhotonEx

Corporation, which developed a 40 Gb/s long-haul optical transport system. Dr. Kesler spent 10 years with the Georgia Tech Research Institute where he led research programs in electromagnetic scattering, antenna arrays, novel antenna structures, and photonic band-gap structures. He holds over 100 patents and has published over 40 technical journal and conference papers. He holds a B.S., M.S., and Ph.D. from the Massachusetts Institute of Technology in Electrical Engineering and Computer Science.



**Johannes Birkendahl** received his B.Sc. and M.Sc. degree in electrical engineering from the Technical University of Munich, Germany, where the focus of his studies layed in energy storages. He is currently working as a tester for the software development of the energy storages at BMW.



**Josef Krammer** received the Dipl.-Ing. degree in electrical engineering from the Department of Electrical and Computer Engineering at the Technical University of Munich, TUM, Germany. He worked as a researcher at the Institute of Circuit Theory and Signal Processing at the TUM where he received the degree of Dr.-Ing. Since 1991 he is working at the BMW Group in different engineering positions for the development of electronics for conventional and electric vehicles.